



Continuous measurement of air-water gas exchange by underwater eddy covariance

Peter Berg, Michael. L. Pace

5

Department of Environmental Sciences, University of Virginia, Charlottesville, Virginia, USA

Correspondence to: Peter Berg (pb8n@virginia.edu)

10 **Abstract.** Exchange of gasses, such as O₂, CO₂, and CH₄, over the air-water interface is an important component in aquatic ecosystem studies, but exchange rates are typically measured or estimated with substantial uncertainties. This diminishes the precision of common ecosystem assessments associated with gas exchanges such as primary production, respiration, and greenhouse gas emission. Here, we use the aquatic eddy covariance technique – originally
15 developed for benthic O₂ flux measurements – right below the air-water interface (~5 cm) to determine gas exchange rates and coefficients. Using an Acoustic Doppler Velocimeter and a fast-responding dual O₂-temperature sensor mounted on a floating platform, the 3D water velocity, O₂ concentration, and temperature are measured at high-speed (64 Hz). By combining these data, concurrent vertical fluxes of O₂ and heat across the air-water interface are derived, and from the
20 former, gas exchange coefficients. Proof-of-concept deployments at different river sites gave standard gas exchange coefficients (k_{600}) in the range of published values. A 40 h long deployment revealed a distinct diurnal pattern in air-water exchange of O₂ that was controlled largely by physical processes (e.g., diurnal variations in air temperature and associated air-water heat fluxes) and not by biological activity (primary production and respiration). This physical control
25 of gas exchange is prevalent in lotic systems and adds uncertainty to common ecosystem assessments of biological activity relying on water column O₂ concentration recordings. For



example, in the 40 h deployment, there was close-to constant river flow and insignificant winds – two main drivers of lotic gas exchange – but we found gas exchange coefficients that varied by several fold. This was presumably caused by vertical temperature-density gradient formation and erosion in the surface water driven by the heat flux into or out of the river that controlled the turbulent mixing. This effect is unaccounted for in widely used empirical correlations for gas exchange coefficients and is another source of uncertainty in gas exchange estimates. The aquatic eddy covariance technique allows studies of air-water gas exchange processes and their controls at an unparalleled level of detail. A finding related to the new approach is that heat fluxes at the air-water interface can, contrary to those typically found in the benthic environment, be substantial and require correction of O₂ sensor readings using high-speed parallel temperature measurements. Fast-responding O₂ sensors are inherently sensitive to temperature changes, and if this correction is omitted, temperature fluctuations associated with the turbulent heat flux will mistakenly be recorded as O₂ fluctuations and bias the O₂ eddy flux calculation.

40

1 Introduction

1.1 Background

Exchange rates of gasses over the air-water interface in rivers, streams, reservoirs, lakes, and estuaries are key parameters for estimating a number of important ecosystem variables (Cole et al. 2010). Gas exchange rates are used to estimate metabolism of aquatic systems (Hanson et al. 2004; Van de Bogert et al. 2007; Van de Bogert et al. 2012), emission of greenhouse gasses like CO₂ and CH₄ to the atmosphere (Cole et al. 2010), and the role of inland and near-shore waters in regional (Billett and Moore 2008) and global (Cole et al. 2007; Bastviken et al. 2011) carbon cycling. As a result, over several decades a tremendous effort among aquatic scientists has focused on understanding and quantifying gas exchange processes at the air-water interface and their controls under naturally occurring field conditions (Whitman 1923; Butman and Raymond 2011; Raymond et al. 2013).

50



55 Multiple state variables and complex physical processes on both sides of the air-water interface control gas exchange (Macintyre et al. 1995; MacIntyre et al. 2010). Despite this complexity, the widely used expression for gas exchange rates was formulated based on a conceptually simple model assuming that gas is transported by molecular diffusion across intact boundary layers, or thin films, found on each side of the interface (Whitman 1923; Liss and Slater 1974):

60

$$J_{air-water} = k(C_{water} - C_{air}) \quad (1)$$

65

where $J_{air-water}$ is the exchange rate, or vertical flux, of the gas (positive upward), C_{water} is the gas bulk concentration below the film on the water-side, C_{air} is the concentration above the film on the air-side, and k is the gas exchange coefficient, often also referred to as the ‘gas transfer velocity’ or ‘piston velocity’. For most gasses, C_{water} and C_{air} are straight forward to measure with modern sensors (Koopmans and Berg 2015; Fritzsche et al. 2017), or calculate from known functions, but the complexity of gas exchange and its many controlling variables is contained in k (Macintyre et al. 1995; McKenna and McGillis 2004; Cole et al. 2010).

70

75

For sparingly soluble gasses such as O_2 , CO_2 , and CH_4 , the ratio between the molecular diffusivity in air and water is on the order of 10^4 . Consequently, the resistance to gas diffusion is associated with the film on the water-side, even if a substantially thicker film is found on the air-side of the air-water interface. This means that in the case of O_2 , C_{air} is simply the saturation concentration of O_2 in water, which is a well-described function of the water temperature and salinity (Garcia and Gordon 1992) and the atmospheric pressure.

80

Turbulence, or turbulent-like motions, that affects or controls the thickness of the film on the water side, and thus the diffusive resistance to gas transport, can originate from both below and above the water. In shallow streams and rivers, this turbulence is typically generated by the water flow over an uneven or rough bottom. Substantial heat loss from the water can similarly result in density driven water motion that erodes the film (Bannerjee and MacIntyre 2004). On the



contrary, in reservoirs, lakes, and estuaries, the turbulence on the water side of the interface is typically generated by wind, which makes wind speed the dominant controlling variable for k for such systems (Marino and Howarth 1993). Despite the fact that typical conditions such as rough weather, surface waves, and rain can rupture the films on the water side, the simple expression for gas exchange (Eq. 1) is still applied, but with k values that are adjusted accordingly (Watson et al. 1991). Keeping these multivariable, highly dynamic, and complex controls in mind, it is evident that determination of representative k values for specific sites is a challenging task.

90

1.2 Formulation of problem

A number of approaches have been used to study and determine values for k . For smaller rivers and streams they include targeted parallel additions of volatile tracers such as propane and hydrologic tracers such as dissolved chloride, where the latter is added to correct for dilution of propane due to hyporheic mixing (Genereux and Hemond 1992; Koopmans and Berg 2015). A common approach for smaller reservoirs and lakes relies on additions of inert tracers, e.g. SF₆ (Wanninkhof 1985; Cole et al. 2010), whereas floating chambers are often deployed in larger rivers, reservoirs, lakes, and estuaries (Marino and Howarth 1993). In a limited number of studies of large reservoirs and lakes, tower-mounted atmospheric eddy covariance systems have been used to measure air-water exchange, and from that, k values were derived (Anderson et al. 1999; Jonsson et al. 2008; Mammarella et al. 2015). Partly motivated by the substantial and often methodologically challenging effort required to measure k at specific sites with any of these approaches, many studies have simply relied on general empirical correlations for k produced by fitting measurements done in other aquatic systems (Raymond and Cole 2001; Borges et al. 2004; Cole et al. 2010). With the exception of atmospheric eddy covariance measurements, none of these approaches represent a direct way of determining k values because they rely on assumptions that often are difficult to assess, or simply not fulfilled. As a result, gas exchange is viewed among aquatic scientists as the primary source of uncertainty in many standard estimates for aquatic systems (Wanninkhof et al. 1990; Raymond and Cole 2001; Raymond et al. 2012).

110



1.3 Scope of work

The aquatic eddy covariance technique for O₂ flux measurements under undisturbed in situ conditions was originally developed for the benthic environment (Berg et al. 2003). The approach has several significant advantages over other flux methods, including its non-invasive nature (Lorrai et al. 2010), high temporal resolution (Rheuban & Berg 2013), and its ability to integrate over a large benthic surface (Berg et al. 2007). As a result, it has been used to measure whole-system fluxes for substrates such as river bottoms (Lorke et al. 2012; Berg et al. 2013), seagrass meadows (Hume et al. 2011; Rheuban et al. 2014), and coral reefs (Long et al. 2013; Rovelli et al. 2015).

Here, we applied the aquatic eddy covariance technique ‘upside down’ right below the air-water interface to measure O₂ fluxes. From them, we derived exchange coefficients for O₂, and then standard gas exchange coefficients (k_{600}). All measurements were done from a floating platform, and because we used a newly developed fast-responding dual O₂-temperature sensor (Berg et al. 2016), we get parallel fluxes of O₂ and thermal energy, or sensible heat. We conducted proof-of-concept tests including deployments at three river sites that were up to 40 hours long.

2 Methods

2.1 Floating measurements platform

All measurements were done from a floating platform with a catamaran-shaped hull (Fig. 1) that was kept at a fixed position at the river sites by two upstream anchors. Due to this setup and the current’s constant pull on the hull, the platform was stationary during deployment. The modular design and the catamaran-shaped hull allow the platform to be collapsed for storage and easy shipment in a standard sturdy Polymer gun case (Pelican Products, USA).

The 3D velocity field was measured with an Acoustic Doppler Velocimeter (ADV) with a cabled sensor head (cabled Vector, Nortek AS, Norway). This type of ADV allowed the sensor head to be



positioned facing upwards (Fig. 1) while recording the velocity field right below the air-water
140 interface (typically ~ 5 cm). Data were collected continuously at a rate of 64 Hz and represent
water velocity values averaged over the ADV's cylindrical measuring volume ($h \sim 1.4$ cm, $\varnothing \sim 1.4$
cm) located 15.7 cm above the sensor head (Fig. 1).

The O_2 concentration was measured with a new fast-responding dual O_2 -temperature sensor
145 (Berg et al. 2016) which, combined with the velocity data, allows for simultaneous fluxes of O_2
and sensible heat to be derived and also instantaneous temperature correction of the O_2 signal.
This sensor was developed specifically for eddy covariance measurements and was designed to
interface with our standard ADVs (Vectors, Nortek AS, Norway) through a single cable supplying
power to the sensor and also transmitting its two outputs, one for O_2 and one for temperature, to
150 the ADV's data logger to be recorded along with velocities to ensure perfect time alignment of all
data. The O_2 measuring part of this new sensor is a small planar optode and concentrations are
determined from fluorescence life-time measurements (Klimant et al. 1995; Holst et al. 1997;
Holst et al. 1998). The sensor tip size, including the temperature thermistor, has a diameter of 8.0
mm which makes it far more robust than O_2 micro-sensors typically used for aquatic eddy
155 covariance measurements and its response times ($t_{90\%}$) were measured to be 0.51 s and 0.34 s for
 O_2 and temperature, respectively (Berg et al. 2016). The edge of the sensor tip was positioned
 ~ 2.0 cm downstream of the edge of the ADV's measuring volume so that water passed through
this volume before sweeping over the angled O_2 sensing tip (Fig. 2a). This setup ensured
undisturbed measurements of the natural current flow. Power was supplied from an external
160 battery (Fig. 1a) with a capacity that allowed 64 Hz data to be collected continuously for at least
48 h. Because all instrument components were designed for underwater use they are not affected
by rain or humid conditions.

Measurement of supporting environmental variables during each deployment allowed
165 verification of recorded data and assisted in the interpretation of the derived eddy fluxes. These
variables included mean O_2 concentration and temperature at the measuring depth recorded



every 1 min with one or two stable independent dual O₂-temperature sensors (miniDOT, PME, USA). In some deployments photosynthetically active radiation (PAR) was also recorded at the measuring depth every 5 min using an independent submersible PAR sensors (Odyssey, Dataflow Systems, New Zealand). For one deployment, light data were taken from nearby meteorological weather stations.

2.2 Field tests

The new approach for determining air-water gas exchange rates and associated exchange coefficients from underwater eddy covariance measurements was tested at three river sites, one in the Hardware River (Virginia) and two in the Mechums River (Virginia). All sites had a fairly linear run with a water depth between ~0.3 and ~1 m and smooth and quietly flowing water (Fig. 1c) without standing riffles or waves. Typical surface flow velocities ranged from 6 to 30 cm s⁻¹. The ADV and the fast-responding O₂-temperature sensor were adjusted to record data ~5 cm below the air-water interface. Four deployments lasting up to 40 h were initiated on November 22, 2015 and September 14, 2016 in the Hardware River and on December 21, 2016 and January 18, 2017 in the Mechums River. Using a level and by placing dive weights on the platform (Fig. 1b) care was taken to ensure that the instrument was as level as possible to minimize post-processing rotations of the velocity field to correct for sensor tilt.

2.3 Calculations of eddy fluxes

Fluxes of O₂ and heat were extracted from the raw eddy covariance data following the same multi-step process briefly described below for O₂. If needed, the O₂ concentration was calibrated against the stable independent dual O₂-temperature sensor data. All 64 Hz data were then reduced to 8 Hz data, which reduces noise while providing sufficient resolution to contain the full frequency spectrum carrying the detectable flux signal (Berg et al. 2009). This assumption was validated by comparing fluxes calculated from both 8 and 64 Hz data for a subset of the data.



O₂ fluxes, one for each 15-min data segment, were extracted from the 8 Hz data using the software
195 package EddyFlux version 3.1 (P. Berg unpubl.). If needed, this software rotates the flow velocity
field for each data segment to correct for any sensor tilt (Lee et al. 2004; Lorrai et al. 2010; Lorke
et al. 2013) bringing the transverse and vertical mean velocities to zero. The vertical eddy flux
was then calculated as (defined positive upward):

200
$$J_{eddy} = \overline{w' C'} \quad (2)$$

where the overbar symbolizes the averaging over the 15-min data segment, and w' and C' are the
fluctuating vertical velocity and the fluctuating O₂ concentration, respectively. These fluctuating
components are calculated as $w - \bar{w}$ and $C - \bar{C}$ where w and C are measured values (at 8 Hz), and
205 \bar{w} and \bar{C} are mean values defined as least square linear fits to all w and C values within the 15-min
time segment, a procedure usually referred to as linear de-trending (Lee et al. 2004; Berg et al.
2009).

Due to the response time of the dual O₂-temperature sensor and its position downstream from the
210 ADV's measuring volume, a time shift correction was applied. This was done by repeating the
outlined flux extraction procedure, while shifting the 8 Hz O₂ concentration data back in time, 1/8
s at a time, until the numerically largest flux was found.

Estimating the gas exchange coefficient requires the O₂ flux over the air-water interface to be
215 known. However, the eddy flux, J_{eddy} , is measured ~5 cm below the interface. By using the linear fit
to the measured O₂ concentrations in each 15-min data segment, defined as \bar{C} above, J_{eddy} is
corrected for storage of O₂ in ~5 cm volume of water to give the flux at the interface:

220
$$J_{eddy, air-water} = J_{eddy} - \int_0^h \frac{d\bar{C}}{dt} dz \quad (3)$$



where h is the ~ 5 cm tall water column. For further details on this flux extraction protocol included in EddyFlux version 3.1, see Lorrai et al. (2010), Hume et al. (2011), and Rheuban et al. (2014). For presentation, the 15-min fluxes were lumped in groups of four to give hourly values.

225 To examine the eddy frequencies that carried the flux signal, for several consecutive data segments in each deployment, cumulative co-spectra of the O_2 concentration and the vertical velocity were calculated using the software package Spectra version 1.2 (P. Berg unpubl.).

2.4 Calculations of gas exchange coefficients

230 The saturation concentration of O_2 (C_{air} in Eq. 1) was calculated from Garcia and Gordon (1992) as a function of salinity (here 0 ppt) and surface water temperature measured with the fast-responding dual O_2 -temperature sensor ~ 5 cm below the air-water interface and then corrected for atmospheric pressure using Henry's law (average sea-level pressure of 1013.25 mbar corrected for elevation). The water column O_2 bulk concentration (C_{water} in Eq. 1) was measured
235 with the same sensor. By substituting $J_{air-water}$ (Eq. 1) with the 15-min values for $J_{eddy, air-water}$ (Eq. 3), a gas exchange rate for O_2 was calculated from Eq. 1 and converted to the standard exchange coefficient, k_{600} , for CO_2 at 20 °C (Jähne et al. 1987; Wanninkhof 1992; Cole et al. 2010). For presentation, the 15-min k_{600} values were lumped in groups of four to give hourly values.

240 3 Results

All four deployments resulted in high-quality time series of the velocity field, the O_2 concentration, and the temperature ~ 5 cm below the air-water interface, and derived from those, air-water fluxes of O_2 and heat, and gas exchange coefficients. These data and their interpretation are presented below.

245

3.1 Data example

For a 40 h long deployment initiated on January 18, 2017 in the Mechums River, the 15-min mean current velocity (Fig. 2a) was relatively constant, averaging 20.5 cm s⁻¹. The O_2 concentration



measured with the fast-responding dual O₂-temperature sensor (Fig. 2b) agreed closely with the
250 concentration recorded with the independent sensor and showed a distinct diurnal pattern.
During most of the first night of the deployment, the O₂ concentration increased linearly (h 19 to h
32), whereas a smaller and non-linear increase that tapered off was measured during the second
night (h 45 to h 56). A diurnal pattern was also seen in the calculated O₂ saturation concentration
(Fig. 2b) reflecting variation in water temperature. The cumulative O₂ flux (Fig. 2c), with each
255 data segment covering a 15-min time interval, had clear linear trends indicating a strong eddy flux
signal in the data. The hourly O₂ flux (Fig. 2d), representing means of four successive 15-min flux
estimates, also exhibited a clear diurnal pattern with a nighttime average uptake by the river of
16.4 mmol m⁻² d⁻¹ for the first night, 9.1 mmol m⁻² d⁻¹ for the second night, and an average daytime
release of 11.1 mmol m⁻² d⁻¹. As observed for the O₂ concentration (Fig. 2b), the hourly O₂ flux
260 differed during the two nighttime periods with a close-to constant flux during the first night and a
flux that tapered off during the second night. The hourly standard gas exchange coefficient (k_{600} ,
Fig. 2e) derived from the hourly O₂ flux (Fig. 2d) and the O₂ concentration difference over the air-
water interface (Fig. 2b) was almost constant over the first night of the deployment with an
average of 3.9 m d⁻¹. After that, k_{600} diminished almost 3-fold to a value of 1.4 m d⁻¹ during the
265 daytime. During the second night, k_{600} tapered off markedly from a level found for the first night
to almost 0.89 m d⁻¹ during the last four h of the deployment. This pattern was unexpected given
the almost constant mean current velocity and insignificant winds (Fig. 2a) and the similar O₂
concentration difference (Fig. 2b) for the two nighttime periods. The pattern suggests that gas
exchange was controlled by a more dominant driver than the river current velocity or winds (see
270 Discussion below).

The parallel results derived from the temperature data measured with the fast-responding dual
O₂-temperature sensor agreed perfectly with the temperature recorded with the stable
independent sensor (Fig. 3b) and had, as with the O₂ concentration, a distinct diurnal pattern. A
275 close-to linear decrease occurred during the first night (h 18 to h 32) whereas a smaller and non-
linear decrease that tapered off was recorded during the second night (h 45 to h 56). During the



280 daytime the temperature increased. Unfortunately, we do not have reliable on-site measurements of the air temperature, but we infer that it, together with shortwave (sunlight during day) and longwave (nighttime) thermal radiation, controlled the recorded water temperature variations (Fig. 3b). The cumulative heat flux (Fig. 3c) had, as for O_2 , clear linear trends indicating a strong flux signal in the data. The hourly heat flux (Fig. 3d) also exhibited a clear diurnal pattern with a nighttime average release of heat of 60.6 W m^{-2} for the first night and 27.5 W m^{-2} for the second night. As was observed for the temperature (Fig. 3b), the hourly heat flux showed different trends for the two nights with a close-to constant flux during the first night and a flux that tapered off
285 during the second night.

Ignoring differences in the sign, representative cumulative co-spectra for the O_2 and heat flux (Fig. 4) during the first night (Figs. 2, 3) were similar in the 0.1 to 1 Hz frequency band with all substantial flux contributions for both the O_2 and heat flux having frequencies lower than $\sim 0.9 \text{ Hz}$.
290 This result, combined with the fast-responding dual O_2 -temperature sensor's response times ($t_{90\%}$) of 0.51 s for O_2 and 0.34 s for temperature (Berg et al. 2016), indicates that the entire eddy flux signal over all frequencies was accounted for in our measurements.

3.2 Representative gas exchange coefficients

295 The three other test deployments were shorter than the one presented in Figs. 2 and 3 but results were of comparable quality. Average values for selected parameters covering periods of time with several successive 15-min time intervals from all four deployments are given in Table 1. These periods were identified by containing consecutive time intervals with consistent standard gas exchange coefficient values, k_{600} , that had little variation and appeared to represent a particular
300 field condition. The longest period ($n = 51$) covers the first full night of the deployment shown in Fig. 2 (h 19 to h 32). Overall, the average current velocity varied from 8.3 to 28.4 cm s^{-1} while k_{600} ranged from 0.4 to 5.1 m d^{-1} , or more than a factor of 12.



305 There was no significant relationship ($r = 0.37$, $p = 0.22$) between river current velocity and k_{600} values (Fig. 5) for all the data in Table 1. Substantial variations in k_{600} values were found for some individual deployments even though the current velocity did not change markedly. Most prominently in the Mechums River deployment, site b (Figs. 2, 3), where the k_{600} values varied more than a factor of 5. As we discuss below, this suggests that, at least for some sites and under some field conditions, other drivers of air-water gas exchange than river flow and winds are more
310 important.

3.3 Temperature effects on O₂ readings – a possible methodological bias

Highly sensitive fast-responding O₂ sensors that can be used for aquatic eddy covariance measurements are inherently sensitive to temperature variations, and thus they will give variable
315 readings at the same molar O₂ concentration if the temperature changes. Typical temperature coefficients (% change in O₂ concentration reading caused by a temperature change of 1 °C) have values of ~3 % (Gundersen et al. 1998). This implies that rapid temperature fluctuations associated with a turbulent heat flux will mistakenly be recorded as fluctuations in O₂ concentration and bias the eddy flux calculation unless a temperature correction of the O₂ reading
320 is performed. In this study, we relied on a new fast-responding dual O₂-temperature sensor (Berg et al. 2016) which puts out rapid simultaneous readings of both the O₂ concentration and the temperature within a distance of few mm and makes this correction possible. This was done for all O₂ fluxes we present. Below, we exemplify the nature and magnitude of this bias if this correction is omitted using data measured during the first night of the deployment depicted in
325 Figs. 2 and 3.

The turbulent temperature fluctuations for a 3-min period shown in Fig. 6a are associated with a vertical heat flux of ~60 W m⁻² (Fig. 3d) and amount to $\pm \sim 0.015$ °C. Based on a temperature coefficient of ~3 %, according to the O₂ calibration equation provided by the producer of our
330 sensor (JFE Advantech, Japan), this translates into fluctuations in O₂ concentration readings of $\pm \sim 0.2$ μmol L⁻¹ (Fig. 6a). Using such ‘simulated’ O₂ data, representing solely temperature sensitivity



effects and produced from the 8 Hz nighttime temperature data (h 18 to h 32, Fig. 3), to calculate an O_2 flux bias gives a release of $11.9 \text{ mmol m}^{-2} \text{ d}^{-1}$ (blue bar, Fig. 6b). Using the temperature corrected O_2 data, as was done for all other calculations we present, gives an oppositely directed O_2 uptake of $16.9 \text{ mmol m}^{-2} \text{ d}^{-1}$ (red bar, Fig. 6b), whereas using the O_2 readings, but without the rapid temperature correction, gives a release of only $4.4 \text{ mmol m}^{-2} \text{ d}^{-1}$ (green bar, Fig. 6b).

4 Discussion

Deploying the aquatic eddy covariance technique right below the air-water interface provided a feasible way to determine gas exchange rates and coefficients. Relative to what is possible with traditional methods, this new approach gives gas exchange rates and coefficients with an improved precision and at a higher spatial and temporal resolution. For those reasons, the approach has the potential to enhance our knowledge on the dynamics and controls of gas exchange and thus benefit aquatic ecosystem studies and pave the way for new lines of ecosystem research.

These points are exemplified in our longest test deployment that lasted 40 h (Figs. 2, 3) and resulted in aquatic eddy covariance data for both O_2 and temperature of a quality and internal consistency that fully match those published for many benthic environments (see review by Berg et al. 2017). Specifically, the 8 Hz velocity, O_2 , and temperature data (Figs. 2a, 2b, 3b) were recorded with low noise and perfectly matched measurements with the stable independent sensor (Figs. 2b, 3b). Furthermore, the cumulative fluxes (Figs. 2c, 3c) had clear linear trends that indicate a strong and consistent flux signal in the data, and the times where the hourly O_2 flux changed direction (Fig. 2d, positive values represent a release), matched exactly the times where the driving O_2 concentration difference changed sign (Fig. 2b). Moreover, the cumulative co-spectra for the O_2 and the temperature fluxes (Fig. 4) have the shape typically seen for shallow-water environments (Lorrai et al. 2010; Berg et al. 2013). Finally, for both O_2 and temperature there was a clear relationship between the flux over the air-water interface (Figs. 2d, 3d) and the observed change in the water column (Figs. 2b, 3b). For O_2 , for example, the ratio between the averaged



360 fluxes for the two nights (h 21 to h 30 vs. h 45 to h 54, Fig. 2d) equals 2.0 which is close to the ratio of 2.2 between the changes in water column concentrations (Fig. 2b) for the same two periods.

Both the O₂ and the temperature data (Figs. 2b, 2d, 3b, 3d) contained a clear diurnal signal overall. For O₂, however, this was not driven by biological processes, i.e. net primary O₂ production during daytime and respiration during nighttime, as this would have resulted in an increase in mean water column O₂ concentration during daytime and a decrease at nighttime. That the opposite pattern was found indicates that physical processes related to thermal conditions were controlling O₂ dynamics. Specifically, colder nighttime air temperatures and possibly also long-wave thermal radiation to the atmosphere were driving the substantial heat flux out of the river (Fig. 3d) which resulted in the falling water temperatures (Fig. 3b). This, in turn, was changing the O₂ saturation concentration (C_{air} in Eq. 1) and thus the driving concentration difference of O₂ exchange over the air-water interface (Fig. 2b). During the daytime, the reverse pattern was in place. This rather complex relationship, or linkage via physical processes, is the only mechanism that can explain the overall pattern found for this deployment (Figs. 2, 3). Considering that these measurements were done under conditions that did not include any uncommon or extreme weather conditions suggests that physical processes, and not biological processes, are often an important, or even the main, driver of O₂ dynamics in shallow-water rivers and streams. An unfortunate consequence of this dominance or control by physical conditions, which we believe is not yet fully recognized, is that it adds substantial uncertainty to the widely used approach of deriving metabolic estimates (e.g., gross primary production, respiration, net ecosystem metabolism) from time series of measured water column O₂ concentrations (Odum 1956; Hall et al. 2016).

385 The standard gas exchange coefficients (k_{600}) for all of our four deployments (distributed on three different river sites, all with smooth quietly flowing water without standing riffles or waves, Fig.1) did not show a significant relationship with river current velocity (Fig. 5, Table 1). This is in line



with previously published results from across-site comparisons (Hall et al. 2016), but the
substantial variation among k_{600} values for some individual deployments (in particular for the
390 'Mechums River, site b' deployment, Figs. 2d) despite only moderately varying river flow velocity
and insignificant winds is surprising. For example, k_{600} varied from a close-to constant value of 3.9
m d⁻¹ during the first night (h 19 to h 32, Fig. 2e), followed by an almost 3 times smaller daytime
value of 1.4 m d⁻¹ (h 33 to h 42), and then increased again at the onset of the second night before
finally tapering off to a small value of 0.9 m d⁻¹ (h 52 to h 56) at the end of the deployment. The co-
395 variance of the heat exchange (Fig. 3d) suggests that turbulence, or turbulent-like motions (which
stimulates gas exchange) was generated by natural convective forces driven by the substantial
heat-loss from the river during the nighttime (Fig. 3d). Conversely, during the daytime, when the
heat flux was directed into the river (Fig. 3d), turbulent motions were presumably dampened by
vertical temperature stratifications in the surface water. Given the 'low-energy' smooth and
400 quietly flowing water, we find this explanation for the varying k_{600} values (Fig. 2e) likely and note
that it has been described before (Bannerjee and MacIntyre 2004; MacIntyre et al. 2010). We also
note that this observed complex pattern illustrates the difficulties that can be associated with
determining accurate air-water gas exchange rates and coefficients without direct site- and time-
specific measurements.

405

An important methodological finding linked to the new approach is that O₂ sensor readings
should, at least in some cases, be corrected using concurrent rapid temperature readings as was
done here for all O₂ fluxes used to estimate air-water gas exchange coefficients (Fig. 2, Table 1). In
the benthic environment where the aquatic eddy covariance technique for O₂ flux measurements
410 was first developed (Berg et al. 2003), the vertical turbulent heat flux is usually small relative to
the O₂ flux due to slowly and modestly varying mean temperatures in the bottom water. At the
air-water interface, however, the heat flux is typically larger due to substantial variations in air
temperatures and short- and long-wave thermal radiation. As a result, rapid temperature
fluctuations associated with the turbulent heat flux below the air-water interface will mistakenly
415 be recorded as fluctuations in the O₂ concentration if this correction is omitted and bias the O₂



flux calculation substantially (Fig. 6). It is unclear how widespread this problem is – more studies are needed to determine that – but in the example included here, this bias alters the flux by more than a factor of 2 (Fig. 6). Our data were recorded during winter, and one could argue that the O₂ exchange would be much larger during summer due to extensive primary production and respiration which would reduce the relative magnitude of this bias (Fig. 6). But as the O₂ flux is indeed likely to be more pronounced during summer than during winter, so is the heat flux.

5 Summary and recommendations

Based on our proof-of-concept deployments, the aquatic eddy covariance technique applied right below the air-water interface should be particularly useful in detailed studies of gas exchange that evaluate its dynamics and controls. The approach can consequently help reduce the generally recognized problem of large uncertainties linked to gas exchange estimates in traditional aquatic ecosystem studies.

The floating platform we used here for measuring aquatic eddy covariance fluxes right below the air-water interface (Fig. 1) can easily be reproduced as it relies exclusively on standard materials and commercially available instrumentation, the latter designed with plug-and-play capabilities. Furthermore, standard software for eddy flux extractions developed for the benthic environment or for the atmospheric boundary layer can be used to estimate air-water fluxes.

We recommend that eddy covariance data are recorded close to the air-water interface (Fig. 1c) to minimize the effects of the O₂ storage in the water between the measuring point and the surface and because gradients of both O₂ and temperature can form in the upper water column. We also recommend that simultaneous rapid temperature measurements are performed within a few mm of the O₂ concentration recordings to allow for temperature corrections of the O₂ signal (Fig. 6).

Finally, our results illustrate that the O₂ concentration difference driving the air-water gas exchange is often small (Fig. 2), here < 2 % of the absolute concentration. This emphasizes the



445 importance of relying both on accurately calibrated sensors to measure the water bulk
concentration (C_{water} in Eq. 1) and precise determinations of the saturation concentration (C_{air} in
Eq. 1) that is corrected for temperature, salinity, and atmospheric pressure.

6 Future work

450 A further development of the new application of the aquatic eddy covariance technique presented
here is to perform similar measurements from a moving platform in small lakes, reservoirs, and
estuaries. In these environments, gas exchange and gas exchange coefficients are expected to vary
spatially, for example from the lee to windward side of the aquatic system. By using a floating
autonomously moving platform, we anticipate that such variations can be spatially mapped out
and studied. We are currently performing the first tests along these lines.

455

7 Acknowledgements

This study was supported by grants from the National Science Foundation (ESC-1550822, OCE-
1334848) and the University of Virginia. We thank Julie and John Baird, Nancy and Ed Mcurdo,
Martha Hodgkins, and Brian Richter who allowed us to work on their beautiful properties in the
460 Hardware River and the Mechums River. Finally, we thank Rachel E. Michaels for editorial
assistance on the manuscript.



8 References

- 465 Anderson, D. E., R. G. Striegl, D. I. Stannard, C. M. Michmerhuizen, T. A. McConnaughey, and J. W.
LaBaugh. 1999. Estimating lake-atmosphere CO₂ exchange. *Limnol. Oceanogr.* **44**: 988-
1001.
- Bannerjee, S., and S. MacIntyre. 2004. The air–water interface: turbulence and scalar interchange.
Advances in coastal and ocean engineering **9**: 181-237.
- 470 Bastviken, D., L. J. Tranvik, J. A. Downing, P. M. Crill, and A. Enrich-Prast. 2011. Freshwater
Methane Emissions Offset the Continental Carbon Sink. *Science* **331**: 50-50.
- Berg, P., M. L. Delgard, R. N. Glud, M. Huettel, C. E. Reimers, and M. L. Pace. 2017. Non-invasive
Flux Measurements at the Benthic Interface: the Aquatic Eddy Covariance Technique. *Limnol.
Oceanogr.*: e-Lectures doi: **10.1002/loe2.10005**.
- 475 Berg, P., D. Koopmans, M. Huettel, H. Li, K. Mori, and A. Wüest. 2016. A new robust dual oxygen-
temperature sensor for aquatic eddy covariance measurements. *Limnol. Oceanogr.*: Methods **14**:
151–167.
- Berg, P., M. H. Long, M. Huettel, J. E. Rheuban, K. J. McGlathery, R. W. Howarth, K. H. Foreman, A.
E. Giblin, and R. Marino. 2013. Eddy correlation measurements of oxygen fluxes in permeable
sediments exposed to varying current flow and light. *Limnol. Oceanogr.* **58**: 1329–1343.
- 480 Berg, P., H. Roy, F. Janssen, V. Meyer, B. B. Jorgensen, M. Huettel, and D. de Beer. 2003. Oxygen
uptake by aquatic sediments measured with a novel non-invasive eddy-correlation technique.
Marine Ecology Progress Series **261**: 75-83.
- Billett, M., and T. Moore. 2008. Supersaturation and evasion of CO₂ and CH₄ in surface waters at Mer
Bleue peatland, Canada. *Hydrological Processes* **22**: 2044-2054.
- 485 Borges, A. V., B. Delille, L. S. Schiettecatte, F. Gazeau, G. Abril, and M. Frankignoulle. 2004. Gas
transfer velocities of CO₂ in three European estuaries (Randers Fjord, Scheldt, and Thames).
Limnol. Oceanogr. **49**: 1630-1641.
- Butman, D., and P. A. Raymond. 2011. Significant efflux of carbon dioxide from streams and rivers in
the United States. *Nature Geoscience* **4**: 839-842.
- 490 Cole, J. J., D. L. Bade, D. Bastviken, M. L. Pace, and M. Van de Bogert. 2010. Multiple approaches to
estimating air-water gas exchange in small lakes. *Limnology And Oceanography-Methods* **8**:
285-293.
- Cole, J. J., Y. T. Prairie, N. F. Caraco, W. H. McDowell, L. J. Tranvik, R. G. Striegl, C. M. Duarte, P.
Kortelainen, J. A. Downing, J. J. Middelburg, and J. Melack. 2007. Plumbing the global carbon
495 cycle: Integrating inland waters into the terrestrial carbon budget. *Ecosystems* **10**: 171-184.
- Fritzsche, E., P. Gruber, S. Schutting, J. P. Fischer, M. Strobl, J. D. Müller, S. M. Borisov, and I.
Klimant. 2017. Highly sensitive poisoning-resistant optical carbon dioxide sensors for
environmental monitoring. *Analytical Methods* **9**: 55-65.
- Garcia, H. E., and L. I. Gordon. 1992. Oxygen solubility in seawater: Better fitting equations. *Limnol.
500 Oceanogr.* **37**: 1307-1312.
- Genereux, D. P., and H. F. Hemond. 1992. Determination of gas exchange rate constants for a small
stream on Walker Branch Watershed, Tennessee. *Water Resources Research* **28**: 2365-2374.



- 505 Gundersen, J. K., N. B. Ramsing, and R. N. Glud. 1998. Predicting the signal of O-2 microsensors from physical dimensions, temperature, salinity, and O-2 concentration. *Limnology & Oceanography* **43**: 1932-1937.
- Hall, R. O., J. L. Tank, M. A. Baker, E. J. Rosi-Marshall, and E. R. Hotchkiss. 2016. Metabolism, gas exchange, and carbon spiraling in rivers. *Ecosystems* **19**: 73-86.
- Hanson, P. C., A. I. Pollard, D. L. Bade, K. Predick, S. R. Carpenter, and J. A. Foley. 2004. A model of carbon evasion and sedimentation in temperate lakes. *Global Change Biology* **10**: 1285-1298.
- 510 Holst, G., R. N. Glud, M. Kuhl, and I. Klimant. 1997. A Microoptode Array For Fine-Scale Measurement of Oxygen Distribution. *Sensors & Actuators B Chemical* **38**: 122-129.
- Holst, G., O. Kohls, I. Klimant, B. Konig, M. Kuhl, and T. Richter. 1998. A modular luminescence lifetime imaging system for mapping oxygen distribution in biological samples. *Sensors and Actuators B-Chemical* **51**: 163-170.
- 515 Hume, A. C., P. Berg, and K. J. McGlathery. 2011. Dissolved oxygen fluxes and ecosystem metabolism in an eelgrass (*Zostera marina*) meadow measured with the eddy correlation technique. *Limnol. Oceanogr.* **56**: 86-96.
- Jähne, B., K. O. Münnich, R. Bösinger, A. Dutzi, W. Huber, and P. Libner. 1987. On the parameters influencing air-water gas exchange. *Journal of Geophysical Research: Oceans* **92**: 1937-1949.
- 520 Jonsson, A., J. Åberg, A. Lindroth, and M. Jansson. 2008. Gas transfer rate and CO₂ flux between an unproductive lake and the atmosphere in northern Sweden. *Journal of Geophysical Research: Biogeosciences* **113**.
- Klimant, I., V. Meyer, and M. Kuehl. 1995. Fiber-optic oxygen microsensors, a new tool in aquatic biology. *Limnol. Oceanogr.* **40**: 1159-1165.
- 525 Koopmans, D. J., and P. Berg. 2015. Stream oxygen flux and metabolism determined with the open water and aquatic eddy covariance techniques. *Limnol. Oceanogr.* **60**: 1344-1355.
- Liss, P., and P. Slater. 1974. Flux of gases across the air-sea interface. *Nature* **247**: 181-184.
- Long, M. H., P. Berg, D. de Beer, and J. C. Zieman. 2013. In situ coral reef oxygen metabolism: An eddy correlation study. *Plos One* **8**: e58581. doi:58510.51371/journal.pone.0058581.
- 530 Lorke, A., D. F. McGinnis, A. Maeck, and H. Fischer. 2012. Effect of ship locking on sediment oxygen uptake in impounded rivers. *Water Resources Research* **48**.
- Lorrai, C., D. F. McGinnis, P. Berg, A. Brand, and A. Wüest. 2010. Application of oxygen eddy correlation in aquatic systems. *Journal of Atmospheric and Oceanic Technology* **27**: 1533-1546.
- 535 MacIntyre, S., A. Jonsson, M. Jansson, J. Aberg, D. E. Turney, and S. D. Miller. 2010. Buoyancy flux, turbulence, and the gas transfer coefficient in a stratified lake. *Geophysical Research Letters* **37**.
- Macintyre, S., R. Wanninkhof, and J. P. Chanton. 1995. Trace gas exchange across the air-water interface in freshwater and coastal marine environments, p. 52-97. *In* R. C. H. P.A. Matson [ed.], *Biogenic Trace Gases: Measuring Emissions from Soil and Water*. Blackwell Science Ltd.
- 540 Mammarella, I., A. Nordbo, Ü. Rannik, S. Haapanala, J. Levula, H. Laakso, A. Ojala, O. Peltola, J. Heiskanen, J. Pumpanen, and T. Vesala. 2015. Carbon dioxide and energy fluxes over a small boreal lake in Southern Finland. *Journal of Geophysical Research: Biogeosciences*: 2014JG002873.
- Marino, R., and R. W. Howarth. 1993. Atmospheric oxygen-exchange in the Hudson River - Dome measurements and comparison with other natural-waters. *Estuaries* **16**: 433-445.



- 545 McKenna, S., and W. McGillis. 2004. The role of free-surface turbulence and surfactants in air–water gas transfer. *International Journal of Heat and Mass Transfer* **47**: 539-553.
- Odum, H. T. 1956. Primary production in flowing waters. *Limnol. Oceanogr.* **1**: 103-117.
- Raymond, P., and J. Cole. 2001. Gas exchange in rivers and estuaries: Choosing a gas transfer velocity. *Estuaries* **24**: 312-317.
- 550 Raymond, P. A., J. Hartmann, R. Lauerwald, S. Sobek, C. McDonald, M. Hoover, D. Butman, R. Striegl, E. Mayorga, C. Humborg, P. Kortelainen, H. Durr, M. Meybeck, P. Ciais, and P. Guth. 2013. Global carbon dioxide emissions from inland waters. *Nature* **503**: 355-359.
- Raymond, P. A., C. J. Zappa, D. Butman, T. L. Bott, J. Potter, P. Mulholland, A. E. Laursen, W. H. McDowell, and N. D. 2012. Scaling the gas transfer velocity and hydraulic geometry in streams and small rivers. *Limnology and Oceanography: Fluids & Environments* **2**: 41-53.
- 555 Rheuban, J. E., P. Berg, and K. J. McGlathery. 2014. Multiple timescale processes drive ecosystem metabolism in eelgrass (*Zostera marina*) meadows. *Marine Ecology Progress Series* **507**: 1–13.
- Rovelli, L., K. M. Attard, L. D. Bryant, S. Flögel, H. J. Stahl, M. Roberts, P. Linke, and R. N. Glud. 2015. Benthic O₂ uptake of two cold-water coral communities estimated with the non-invasive eddy-correlation technique. *Marine Ecology Progress Series* **525**: 97-104.
- 560 Van de Bogert, M. C., D. L. Bade, S. R. Carpenter, J. J. Cole, M. L. Pace, P. C. Hanson, and O. C. Langman. 2012. Spatial heterogeneity affects estimates of ecosystem metabolism in two northern lakes. *Limnol. Oceanogr.* **57**: 1689-1700.
- Van de Bogert, M. C., S. R. Carpenter, J. J. Cole, and M. L. Pace. 2007. Assessing pelagic and benthic metabolism using free water measurements. *Limnology And Oceanography-Methods* **5**: 145-155.
- 565 Wanninkhof, R. 1985. Kinetic fractionation of the carbon isotopes ¹³C and ¹²C during transfer of CO₂ from air to seawater. *Tellus B* **37**: 128-135.
- . 1992. Relationship between wind speed and gas exchange over the ocean. *Journal of Geophysical Research: Oceans* **97**: 7373-7382.
- 570 Wanninkhof, R., P. J. Mulholland, and J. W. Elwood. 1990. Gas-exchange rates for a 1st-order stream determined with deliberate and natural tracers. *Water Resources Research* **26**: 1621-1630.
- Watson, A. J., R. C. Upstill-Goddard, and P. S. Liss. 1991. Air–sea gas exchange in rough and stormy seas measured by a dual-tracer technique. *Nature* **349**: 145-147.
- 575 Whitman, W. G. 1923. The two film theory of gas absorption. *Chemical and Metallurgical Engineering* **29**: 146-148.



9 Tables

Deployment	Start date	<i>n</i>	Current velocity cm s ⁻¹	O ₂ flux mmol m ⁻² d ⁻¹	<i>k</i> ₆₀₀ m d ⁻¹
-	-	-			
Hardware River, dep. 1	Nov 22, 2015	20	28.4	9.1	1.6
"	"	39	27.5	12.0	2.7
"	"	13	27.6	-10.7	2.5
Hardware River, dep. 2	Sep 14, 2016	20	8.7	7.0	0.4
"	"	4	8.3	9.4	0.7
Mechums River, site a	Dec 21, 2016	23	9.4	-42.9	2.3
"	"	36	9.3	-29.2	1.7
Mechums River, site b	Jan 18, 2017	4	25.6	-8.9	1.9
"	"	51	18.4	16.8	3.9
"	"	34	20.4	-11.8	1.3
"	"	3	22.9	19.3	5.1
"	"	16	23.4	10.1	2.1
"	"	26	21.3	5.8	1.0

Table 1: Representative standard gas exchange coefficients (*k*₆₀₀) along with current velocity and O₂ flux for four deployments at three different sites. The third column (*n*) specifies the number of 15-min time intervals included in the averages. Values from the last deployment (Mechums River, site b) are depicted in Figs. 2 and 3.



10 Figures



Figure 1: Floating platform for determining air-water gas exchange. **(a)** The 120 cm long and 90 cm wide platform with a catamaran-shaped hull being prepared for deployment. Four inflatable fenders provide flotation. **(b)** The platform deployed in the Hardware River and anchored to both river banks. A dive weight is used to level the platform. **(c)** Close-up look at the ADV's three-pronged upward-facing sensor head and the fast-responding dual O₂-temperature sensor. Two stable independent dual O₂-temperature sensors used for calibration are seen to the far right.

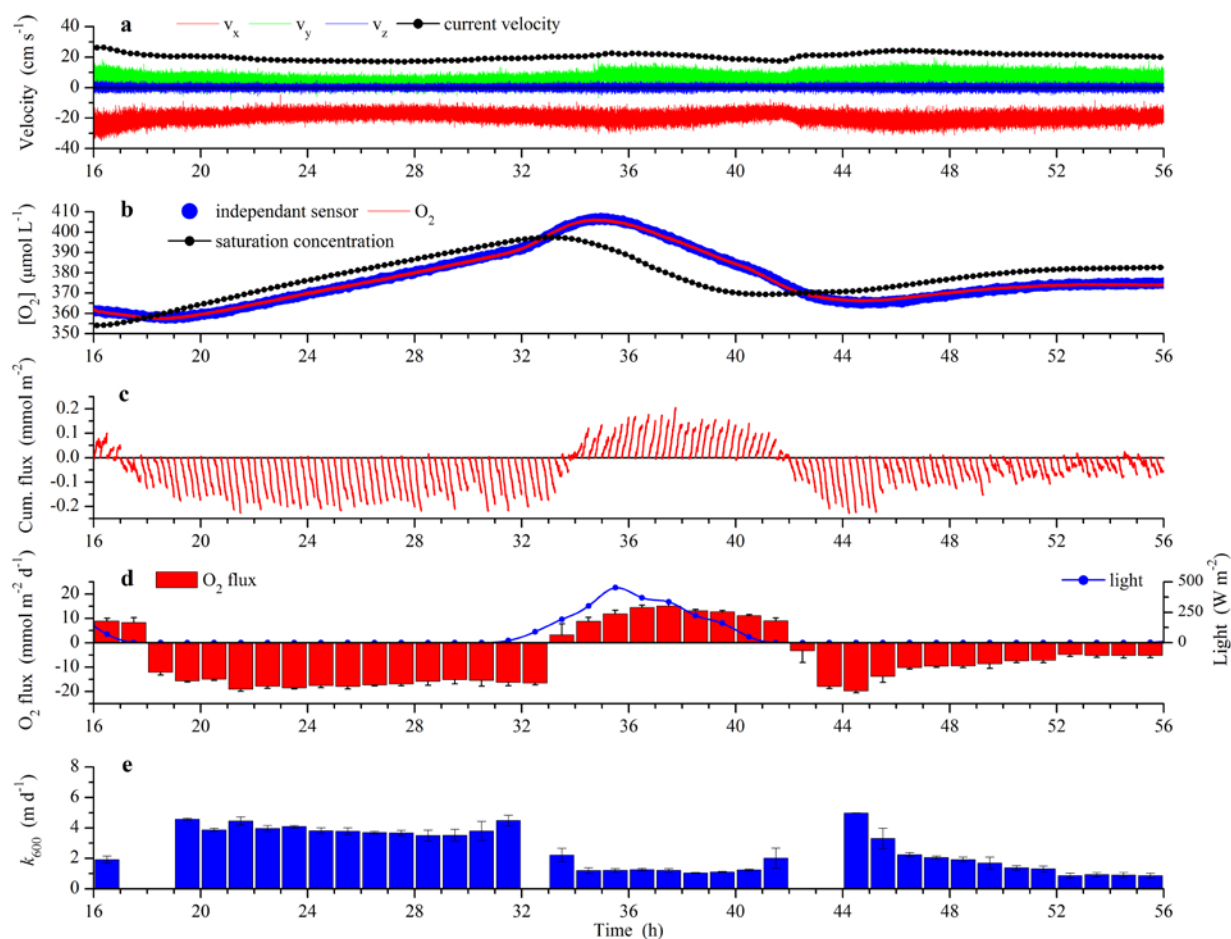


Figure 2: Forty h long test deployment initiated at 16:00 in the afternoon as indicated on the x-axis. **(a)** Three velocity components at 8 Hz (x, y, z ; z is vertical) and 15-min mean current velocity. **(b)** O_2 concentration at 8 Hz measured with the dual O_2 -temperature sensor and at 1-min measured with an independent sensor. **(c)** Cumulative flux over 15-min time intervals with clear linear trends. **(d)** Hourly O_2 flux (positive values represent a release from the river), each value based on 15-min flux extractions ($n = 4$, SE) and day light measured at a nearby weather station. **(e)** Hourly standard gas exchange coefficient (k_{600}) based on 15-min estimates ($n = 4$, SE). The few gaps in the data are for the times where the driving O_2 concentration difference changes sign (panel c).

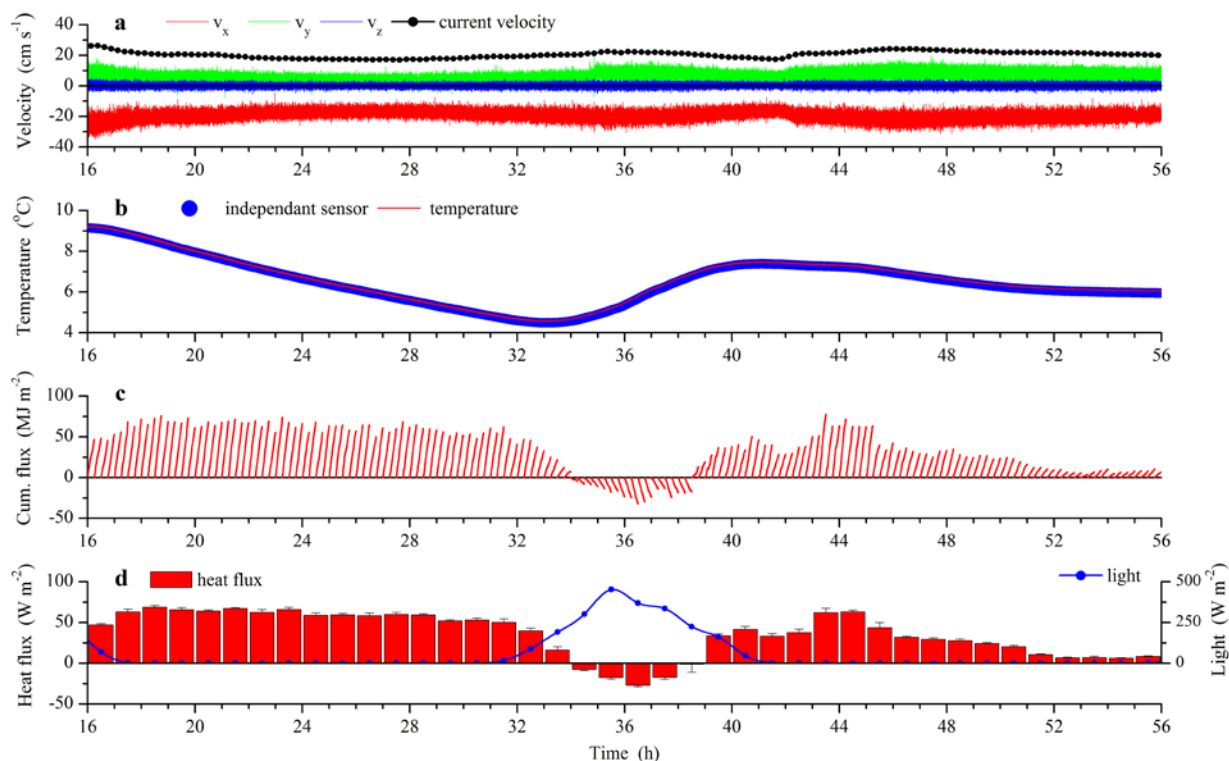


Figure 3: Same deployment as in Fig. 2, but with results for temperature and heat. The deployment was initiated at 16:00 in the afternoon as indicated on the x-axis. **(a)** Three velocity components at 8 Hz (x, y, z ; z is vertical) and 15-min mean current velocity. **(b)** Temperature at 8 Hz measured with the dual O₂-temperature sensor and at 1-min measured with an independent optode. **(c)** Cumulative flux over 15-min time intervals with clear linear trends. **(d)** Hourly heat flux, each value based on 15-min flux extractions ($n = 4$, SE) and day light measured at a nearby weather station. Positive flux values represent a release of heat from the river.

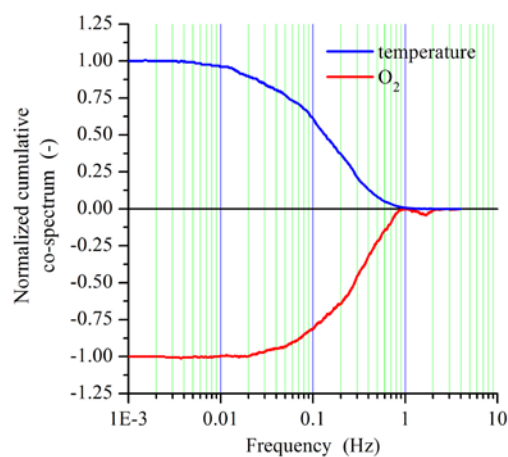


Figure 4: Nighttime normalized cumulative co-spectra for the vertical velocity combined with the O₂ concentration and the temperature, respectively, revealing which frequencies carried the eddy flux signal.

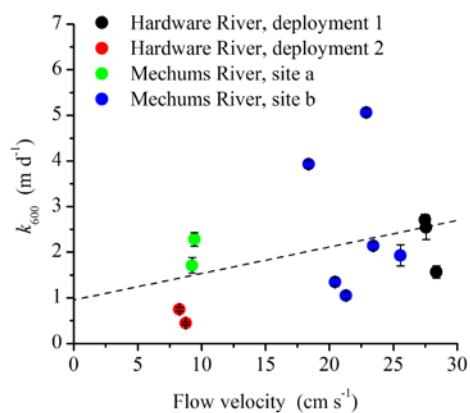


Figure 5: Standard gas exchange coefficient, k_{600} , plotted against river current velocity. The dotted line is a linear fit to all data ($R = 0.37$, $p = 0.22$).

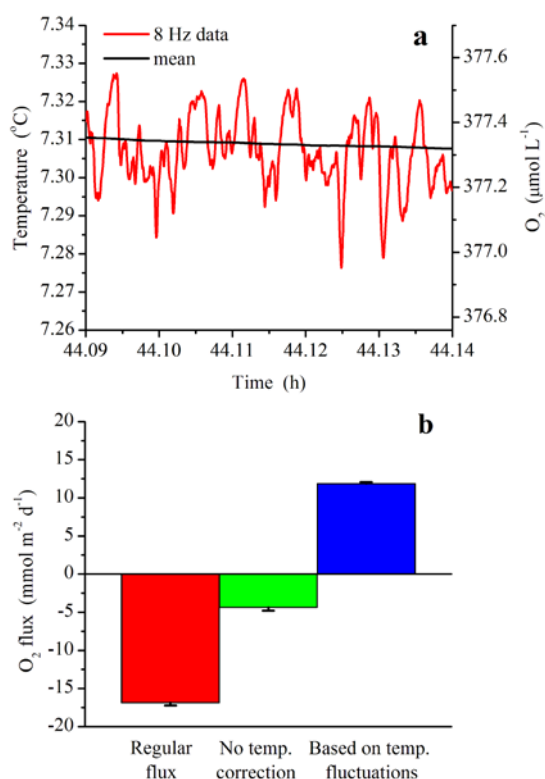


Figure 6: Bias that can arise if O₂ concentration sensor readings are not corrected using rapid parallel temperature measurements. **(a)** Recorded 8 Hz data of temperature fluctuations and their mean (left axis) through 3-min and the resulting fluctuations in O₂ concentration that would be recorded by a sensor with a temperature coefficient of 3 % (right axis). **(b)** Average air-water fluxes, all for the first night (h 18 to h 32) of the deployment depicted in Figs. 2 and 3, calculated using temperature corrected data (red bar), data without rapid temperature correction (green bar), and ‘simulated’ data produced from rapid temperature recordings as shown in panel a and assuming a temperature coefficient of 3 % (blue bar).